Supporting Information

Radu, Schoenwetter et al.

Production of the p34hs(1-233)/p44hs(321-395) complex. The human p34(1-233) and p44(321-395) cDNAs were inserted into the pET28b (Novagen) and the pGEX (GE Healthcare) vectors using sequence and ligation independent cloning (SLIC) (1) and verified by sequencing. The p34hs(1-233) construct harbors an N-terminal cleavable hexa-histidine tag and p44hs(321-395) a GST-cleavable tag. Wild type and mutant (p34hs-R146E or p44hs-F374E) recombinant proteins were co-expressed in *E. coli* BL21 (DE3) cells. Cells were grown in LB medium at 37 °C and protein expression was induced with 0.5 mM isopropyl-β-thiogalactoside after an OD_{600} of 0.7 – 0.8 was reached. Cells were further grown for 20 h at 18 °C, harvested and disrupted by sonication in buffer A (20 mM Tris-HCl pH 8, 250 mM NaCl and 1 mM DTT) containing 10 mM imidazole in the presence of an EDTA-free protease inhibitor cocktail (Complete™, Merck) and then clarified by centrifugation at 40,000 x g for 1 h at 4 °C. The clarified lysate was applied to a Ni-metal affinity resin column (5 ml His-Trap HP, GE Healthcare) and, after washing with buffer A containing increasing imidazole concentrations (10 mM, 25 mM and 75 mM), the bound His-p34hs(1-233)/GST-p44hs(321-395) complex was eluted in the same buffer containing 250 mM imidazole. Next, the complex was applied to a GST affinity resin column (Glutathione sepharose 4B, GE Healthcare). After extensive washing in buffer A, the His- and GST-tags were cleaved from both p34 and p44 using bovine thrombin. The complexes were finally purified by size exclusion chromatography (HiLoad 16/60 Superdex s200pg, GE Healthcare) (Figure S4, A and B) in buffer A containing 2 mM TCEP instead of DDT. The wild type p34hs/p44hs sample was further concentrated to 10 mg/ml using Vivaspin filtration units (Sartorius).

Production of the p34ct(1-277)/p44hs(368-534) complex. The genes encoding p34ct(1-277) and p44ct(368-534) were cloned from a cDNA library from *C. thermophilum* (provided by Ed Hurt). Using SLIC, p34ct(1-277) and p44ct(368-534) were cloned into the pBADM-11 vector (EMBL-Heidelberg) and the pETM-11 vector (EMBL-Heidelberg), respectively. p34ct(1-277) and p44ct(368-534) mutants were generated by site-directed mutagenesis and verified by sequencing (Eurofins Genomics or Seqlab). For co-expression of the wild-type proteins

p34ct(1-277) was expressed with an N-terminal hexa-histidine tag whereas p44ct(368-534) was expressed without any tag. For single protein expression the wild-type proteins as well as all variants were expressed with an N-terminal hexa-histidine tag. Protein expression was carried out in *E. coli* BL21-CodonPlus (DE3) RIL cells (Stratagene). Cells were grown in LB medium at 37 °C and protein expression was induced with 0.05% L-(+)-arabinose (for expression of the p34 variants) or 0.5 mM isopropyl-β-thiogalactoside (for expression of the p44 variants) or with both (for co-expression of wild-type p34 and p44) after an OD_{600} of 0.6 – 0.8 was reached. Cells were further grown for 20 h at 15 °C, harvested and lysed in a buffer containing 20 mM Tris-HCl pH 7.5, 500 mM KCl and 0.5 mM TCEP using a mechanical cell disrupter (Microfluidics). After centrifugation at 38,000 x g for 1 h at 4 °C all proteins were purified using Ni-metal affinity chromatography (Ni-TED, Macherey-Nagel) followed by size exclusion chromatography (HiLoad 16/60 Superdex s200pg, GE Healthcare). Elution of the proteins during affinity chromatography was achieved with a buffer containing 20 mM Tris-HCl pH 8.0, 300 mM KCl, 250 mM imidazole and 1 mM TCEP. Size exclusion chromatography was carried out in either 20 mM CHES pH 9.5 (for co-purification of p34ct(1-277) and p44ct(368-534)) or 20 mM Tris-HCl pH 8.0 (for single purification of p34ct(1-277) or p44ct(368-534)), 150 mM KCl and 1 mM TCEP. The samples were concentrated to 5 – 10 mg/ml, based on their calculated extinction coefficients using ProtParam (SwissProt), via Amicon ultra centrifugal filters (Merck Millipore) and flash frozen in liquid nitrogen for storage at – 80 °C.

The ct sequences of p34 and p44 contain flexible linker insertions that are quite prominent in the ct proteins but are missing in the human proteins and have previously also been described for the p34ct vWA structure (1). The most prominent linker region in p44ct is reaching from residues 410 to 468 and is not visible in the electron-density map of the p34ct/p44ct minimal complex I. To improve crystal packing of the ct p34/p44 minimal complex this flexible linker region in p44ct(368-534) was replaced by five amino acids, namely S-N-G-N-G (ct p34/p44 minimal complex II). The artificial linker was introduced into p44ct(368-534) using SLIC and verified by sequencing. Protein expression and purification was performed as described above.

Structure determination and analysis.

Determination of the p34ct(1-277)/p44ct(386-586) structure. The ct p34/p44 minimal complex I was crystallized at 20°C in 15% (w/v) PEG 20,000 and 100 mM MES pH 6.5, whereas the ct p34/p44 minimal complex II (see *Production of the p34ct(1-277)/p44hs(368-534) complex* section for further information) was crystallized at 20°C in 5 – 10% (w/v) PEG 4,000, 20 – 33% (v/v) MPD and 100 mM HEPES pH 7.0 – 7.5. Crystals of the ct p34/p44 minimal complexes I and II were crystallized at protein concentrations of 5 – 10 mg/ml using the vapor diffusion method in sitting drops. Crystals of complex I used for structure solution took several weeks to grow but failed reproduction. Crystals of complex II were well reproducible and usually took five to ten days to appear. For data collection all crystals were washed in a drop containing the mother liquor supplemented with 20% (v/v) glycerol before they were flash frozen in liquid nitrogen. Data collection of complexes I and II was performed at 100 K and wavelengths of 0.8726 Å and 0.97625 Å at beamlines ID23-2 and BM14 (ESRF), respectively. The data sets were processed using either iMOSFLM and SCALA (2, 3) or XDS and AIMLESS (4, 5). Both complexes crystallized in space group $P6_322$ with one copy of the heterodimer per asymmetric unit but varied in the unit cell dimensions (Table 1). As high resolution cutoff we have chosen a CC1/2 value of 0.6 for all data sets.

The structure of complex I was solved by molecular replacement via Phaser (6) using the structure of the p34ct vWA domain (PDB: 4PN7,(1)) as a search model. The p44ct RING domain was built into the electron density by using the human p44 NMR structure (PDB: 1Z60, (7)) and the weak anomalous signal of the two zinc ions as a guide. Model building and adjustment was performed in Coot (8). The final model of complex I was obtained using the higher resolution model of complex II after the latter had been fully refined. The structure of complex I was refined to a resolution of 3.7 Å with an R-factor of 19.6% and R_{free} of 24.6% using REFMAC (9). This model contains 200 out of 277 residues of the p34ct vWA domain and 74 out of 167 residues of the p44ct RING domain. The structures of complex I and II do not show any significant differences (Figure S9) so that we exclusively discuss the higher resolution complex II model in this study.

The structure of complex II was solved by molecular replacement via Phaser using the structure of complex I as a search model. The structure was refined to a resolution of 2.2 Å

with an R-factor of 21.0% and R_{free} of 22.7% using Phenix refine (10) and REFMAC5. The model was adjusted with Coot. The final model contains residues 18 – 89, 104 – 166 and 198 – 274 (212 out of 277 residues) of p34ct with residues 1 – 17, 90 – 103, 167 – 197 and 275 – 277 being presumably disordered. Taking into account that the artificial linker of p44ct could be modeled, the final model comprises residues 380 – 507 of p44ct (74 out of 113 residues in the improved model) with residues 368 – 379 and 508 – 534 being disordered.

Determination of the p34hs(1-233)/p44hs(321-395) structure. Crystals of the human p34(1-233)/p44(321-395) complex were washed for 30 s in a crystallization solution supplemented with 20% (v/v) PEG 400 or glycerol prior to freezing in liquid nitrogen. X-ray data were collected at 100 K using the PROXIMA1 beam line of the Soleil synchrotron facility (Gif-sur-Yvette, France) and the ID29 beamline of European Synchrotron Radiation Facility (ESRF, Grenoble, France). Data were indexed and integrated using XDS (4); crystals belong to space group $I2_12_12_1$ (R_{merge} of 13.3% and I B (Wilson) of 110 $Å^2$) with two complexes in the asymmetric unit (Table 1).

The structure was determined by molecular replacement using the p34ct vWA domain (PDB: 4PN7) as search model in the CCP4 software suite PHASER and the intrinsic Zn anomalous scattering signal of the two zinc ions in the p44 RING C-terminal domain was used to position this domain. The structure was extended and completed by iterative manual building in Coot (8) and refinement using Phenix (10) using the p34ct/p44ct structure as a guide (Table 1). The asymmetric unit contains two heterodimers: the model of the first complex is composed of 190 (out of 233) and 49 residues (out of 74) for p34hs and p44hs, respectively (chains A and B); the second complex is composed of 192 residues for p34 and 54 residues for p44 (chains C and D; see Figure 2B). Within each dimer, the relative orientation of the p34 and p44 subunits is identical to that observed in the complex from ct, which results in an overall RMSD of 1.5 Å for the 236 equivalent Cα (182 for p34 and 54 for p44).

Interfaces were analysed using PDBsum (11) and PISA (12).

Characterization of protein complexes.

Isothermal titration calorimetry. Thermodynamic parameters of molecular interactions between p34ct(1-277) and p44ct(368-534) were determined by isothermal titration calorimetry (ITC) using a VP-ITC instrument (MicroCal, GE Healthcare) at 37 °C and 260 rpm. All samples were degassed prior to the experiment and equilibrated in the same buffer conditions consisting of 20 mM CHES pH 9.5, 150 mM KCl and 1 mM TCEP. In all experiments, 40 – 50 µM wild-type or mutated p44ct(368-534) were titrated into the sample cell containing 4 – 5 µM wild-type or mutated p34ct(1-277). A volume of 10 µL was added at a time, resulting in 30 injections. The data were analyzed with a single-site binding model using the Origin software (OriginLab). All experiments were repeated at least twice. Control experiments were performed in which p44ct(368-534) was titrated into buffer.

Size exclusion chromatography. Analysis of the interaction between ct wild-type and mutant p34 and p44 proteins was also performed via analytical size exclusion chromatography (SEC) using a Superdex 200 10/300 GL or a Superdex 200 Increase 10/300 GL column (GE Healthcare). All SEC runs were performed in 20 mM Tris-HCl pH 8.0, 150 mM KCl and 1 mM TCEP. 400 µL of a solution containing 12 µM protein was applied onto the column either alone or after mixing the two proteins in a 1:1 ratio and subsequent incubation on ice for 1 h. During sample application and elution at a flow rate of 0.5 mL/min the proteins were detected at 280 nm. Fractions of 0.5 mL were collected during the elution and analyzed via SDS-PAGE. Reference runs with wild-type proteins were always performed prior to runs with mutated proteins.

Circular dichroism spectroscopy. All measurements were performed in a 1 mm quartz cuvette employing a J-715 spectropolarimeter (Jasco) at wavelengths from 260 to 190 nm and room temperature. All samples were equilibrated in the same buffer conditions consisting of 20 mM K_2H/H_2K-PO_4 pH 8.1. To optimize the signal to noise ratio a total of 10 spectra were accumulated. The spectrum of the reference buffer was subtracted from each sample spectrum.

p34hs/p44hs interaction assays. Wild-type or mutated p34hs/p44hs complexes were expressed by infecting *Sf21* insect cells (50 mL) with the appropriate baculoviruses and were resuspended in 25 mL of buffer A. Cell extracts were prepared as described above. Pull down

experiments were performed in buffer B (20 mM Tris-HCl pH 8.0, 250 mM NaCl, 0.1% (v/v) Nonidet P-40, 1 mM TCEP) using 50 µL of Protein A Sepharose cross-linked with 1H5 anti-p44 antibody (directed against residues 1–17 of human p44) (Sigma) or StrepTactin Sepharose (IBA) for p34 pull downs. After extensive washing and equilibration in buffer B, proteins were eluted by competition with 2 column volumes (CV) of buffer B containing the appropriate synthetic peptide at 0.5 mg/mL for immunoprecipitations or 5 mM d-desthiobiotin (Sigma) for elution from StrepTactin Sepharose (IBA) and analyzed on a SDS-PAGE followed by Coomassie staining or by high resolution protein electrophoresis using the LabChip GXII System (Caliper, LifeSciences). The histograms represent the estimated ratios (in arbitrary units, au) between p34hs (wild-type and variants) and p44hs (wild-type and variants).

Protein melting point analysis. Protein thermal stability was measured utilizing a label-free fluorimetric analysis and the Prometheus NT.48 (NanoTemper Technologies). Briefly, the shift of the intrinsic tryptophan fluorescence of proteins upon temperature-induced unfolding was monitored by detecting the emission fluorescence at 330 and 350 nm. Thermal unfolding was performed in nanoDSF grade high-sensitivity glass capillaries (NanoTemper Technologies) at a heating rate of 1 °C per minute. Protein melting points (T_m) were calculated from the first derivative of the ratio of tryptophan emission intensities at 330 and 350 nm. Measurements were performed at constant concentrations of 50 nM of the purified complexes in 20 mM Tris-HCl pH 8, 250 mM NaCl and 1 mM DTT.

References:

1. Schmitt DR, Kuper J, Elias A, Kisker C. The structure of the TFIIH p34 subunit reveals a von Willebrand factor A like fold. PLoS One. 2014;9(7):e102389.
2. Battye TG, Kontogiannis L, Johnson O, Powell HR, Leslie AG. iMOSFLM: a new graphical interface for diffraction-image processing with MOSFLM. Acta Crystallogr D Biol Crystallogr. 2011;67(Pt 4):271-81.
3. Evans P. Scaling and assessment of data quality. Acta Crystallogr D Biol Crystallogr. 2006;62(Pt 1):72-82.
4. Kabsch W. Xds. Acta Crystallogr D Biol Crystallogr. 2010;66(Pt 2):125-32.
5. Evans PR, Murshudov GN. How good are my data and what is the resolution? Acta Crystallogr D Biol Crystallogr. 2013;69(Pt 7):1204-14.
6. McCoy AJ, Grosse-Kunstleve RW, Adams PD, Winn MD, Storoni LC, Read RJ. Phaser crystallographic software. J Appl Crystallogr. 2007;40(Pt 4):658-74.

7. Kellenberger E, Dominguez C, Fribourg S, Wasielewski E, Moras D, Poterszman A, et al. Solution structure of the C-terminal domain of TFIIH P44 subunit reveals a novel type of C4C4 ring domain involved in protein-protein interactions. J Biol Chem. 2005;280(21):20785-92.
8. Emsley P, Lohkamp B, Scott WG, Cowtan K. Features and development of Coot. Acta Crystallogr D Biol Crystallogr. 2010;66(Pt 4):486-501.
9. Murshudov GN, Skubak P, Lebedev AA, Pannu NS, Steiner RA, Nicholls RA, et al. REFMAC5 for the refinement of macromolecular crystal structures. Acta Crystallogr D Biol Crystallogr. 2011;67(Pt 4):355-67.
10. Adams PD, Afonine PV, Bunkoczi G, Chen VB, Davis IW, Echols N, et al. PHENIX: a comprehensive Python-based system for macromolecular structure solution. Acta Crystallogr D Biol Crystallogr. 2010;66(Pt 2):213-21.
11. de Beer TA, Berka K, Thornton JM, Laskowski RA. PDBsum additions. Nucleic Acids Res. 2014;42(Database issue):D292-6.
12. Krissinel E, Henrick K. Inference of macromolecular assemblies from crystalline state. J Mol Biol. 2007;372(3):774-97.

SI Figures and Tables

Figure S1 Comparison of the p34 vWA/p44 RING domain with the UbcH5b~Ub/Ark2C RING complex.

Figure S2: Circular Dichroism analysis p34ct vWA and p44ct RING variants

Figure S3: Mutational analysis of the p34ct/p44ct interface

Figure S4: Mutational analysis of the p34hs(1-233)/p44hs(321-395) interface

Figure S5: Mutational analysis of the interface between full length p34hs/p44hs

Figure S6: Stability of the p34/p44 heterodimer and HDMX analysis

Figure S7: C4 domain model of p34hs

Figure S8: Influence of the p34hs C-terminal domain on the integrity of TFIIH.

Figure S9: Overall superposition of the p34ct/p44ct complex I and the p34ct/p44ct complex II

***Table S1*.** Representative X-ray and NMR structures of TFIIH components

***Table S2*.** Interface alignment of Human and Ct p34 residues

Table S3. Interface alignment of Human and Ct p44 residues

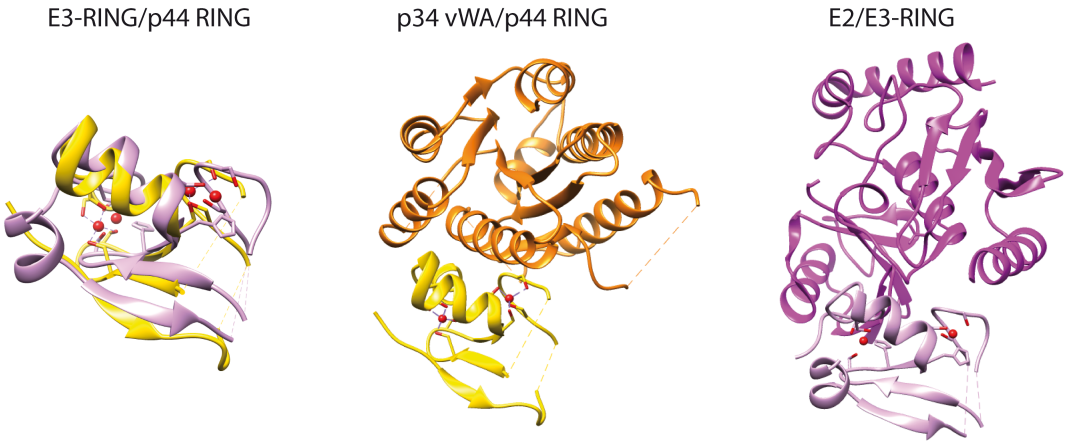

Figure S1 Comparison of the p34 vWA/p44 RING domain with the UbcH5b~Ub/Ark2C RING complex. A superposition of the p44 RING (yellow) with the Ark2C E3 RING (plum) is shown on the left. The p34hs/p44hs minimal complex (p34hs vWA/p44hs RING in orange and yellow, respectively) and the UbcH5b~Ub/Ark2C RING complexes (E2/E3 RING in magenta and plum, respectively) are displayed side by side in the same orientation.

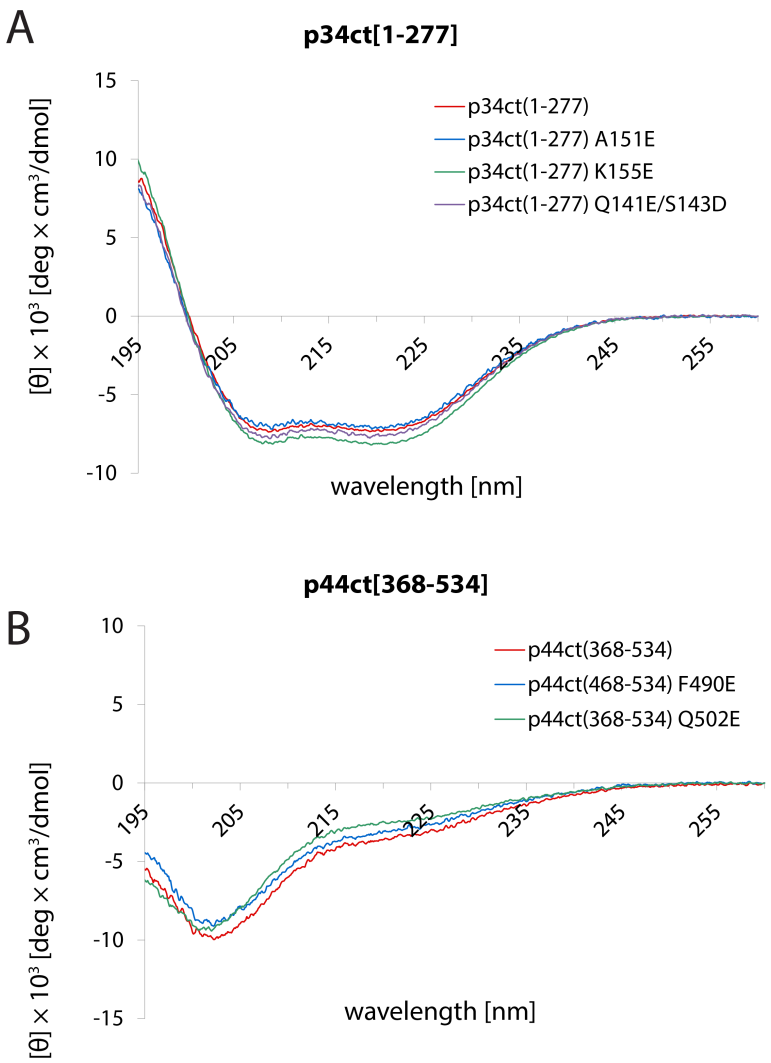

Figure S2: Circular Dichroism spectroscopy of p34ct(1-277) wild-type and variants **(A)** and p44ct(368-534) wild-type and variants **(B).**

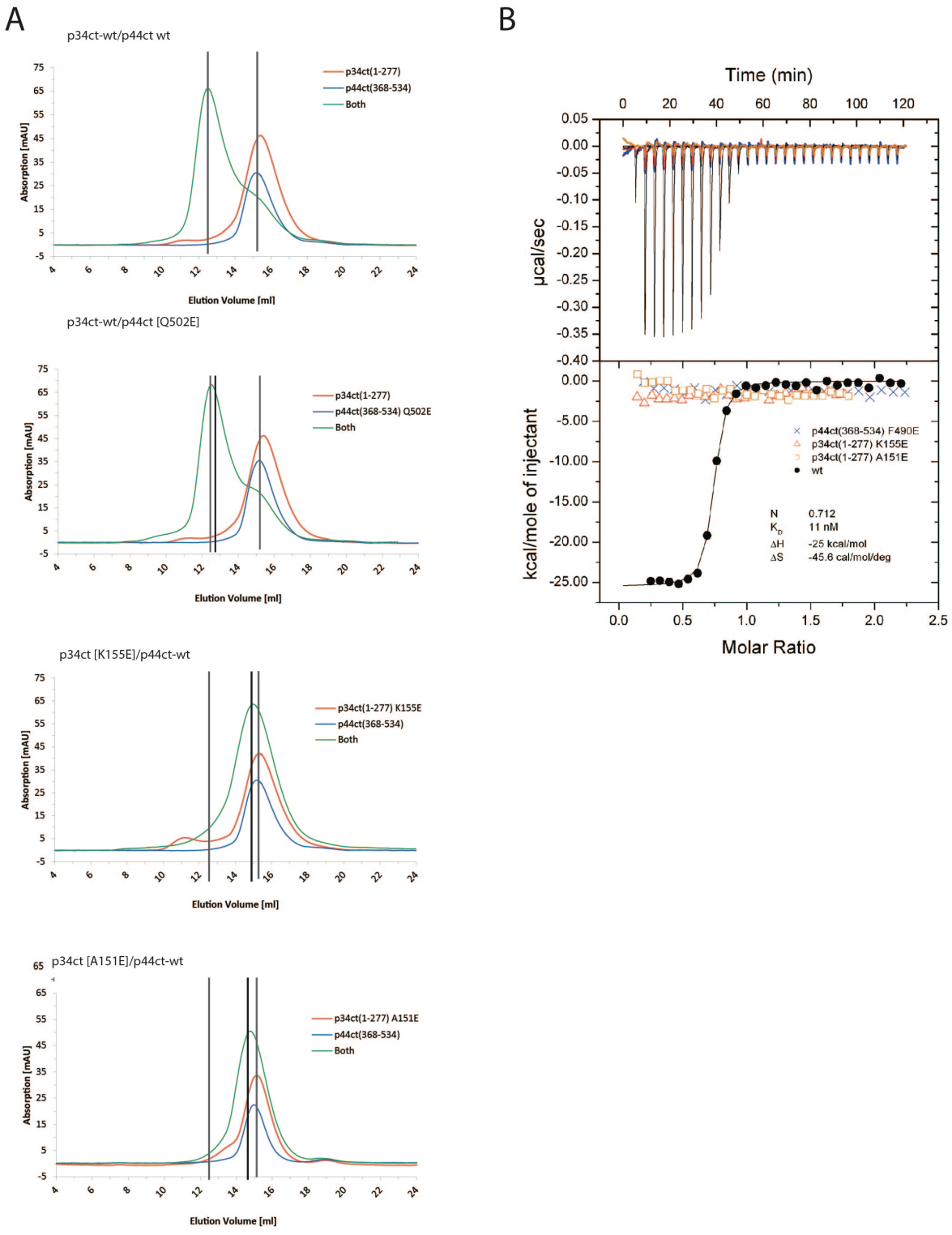

Figure S3: Mutational analysis of the p34ct/p44ct interface from size exclusion chromatography and ITC of wild-type and mutant complexes. **(A)** SEC of p34ct(1-277) with p44ct(368-534) wild-type or variants. p34ct(1-277) (red) and p44ct(368-534) (blue) were analyzed separately and in a 1:1 stoichiometry (green) mixed prior to SEC. **(B)** Quantification of the interaction between wild-type or variant p34ct(1-277) and p44ct(368-534) by ITC. The thermodynamic parameters for the association of the wild-type protein domains are: K_D=11 nM, n=0.71, ΔH=-25 kcal/mol and ΔS=-45 cal/mol/degree.

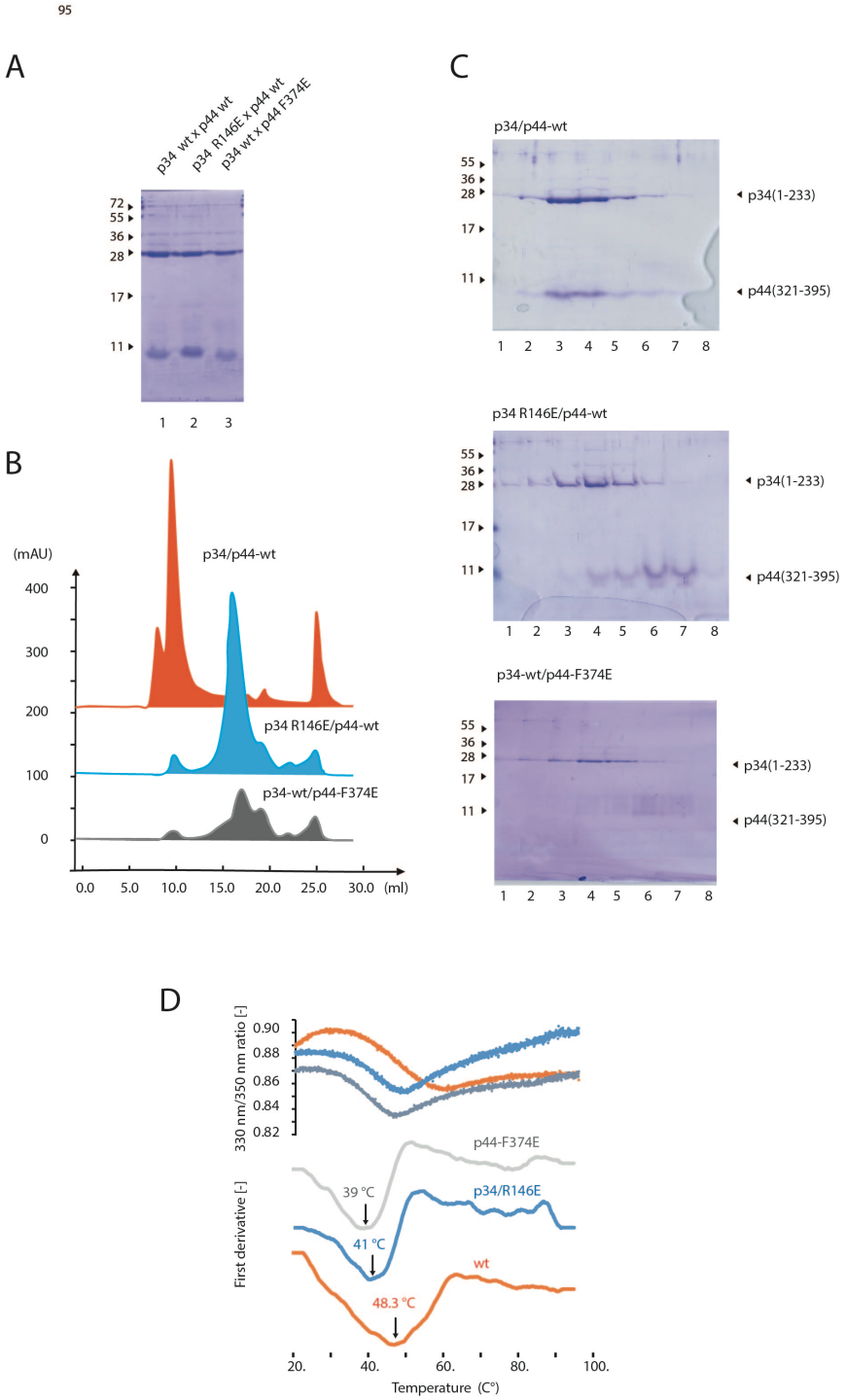

Figure S4: Mutational analysis of the p34hs(1-233)/p44hs(321-395) interface from size exclusion chromatography of wild-type and mutant complexes. The p34hs(1-233)/p44hs(321-395) wild type complex, the p34hs-R146E and the p44hs-F374E variants were co-expressed in *E. coli* and purified using nickel affinity chromatography followed by a GST pull-down. Eluates from the GST-affinity purification step were analysed via SDS-PAGE **(A)**, loaded on a Superdex S200 16/60 gel filtration column **(B and C)** or subjected to a thermal stability analysis **(D)**.

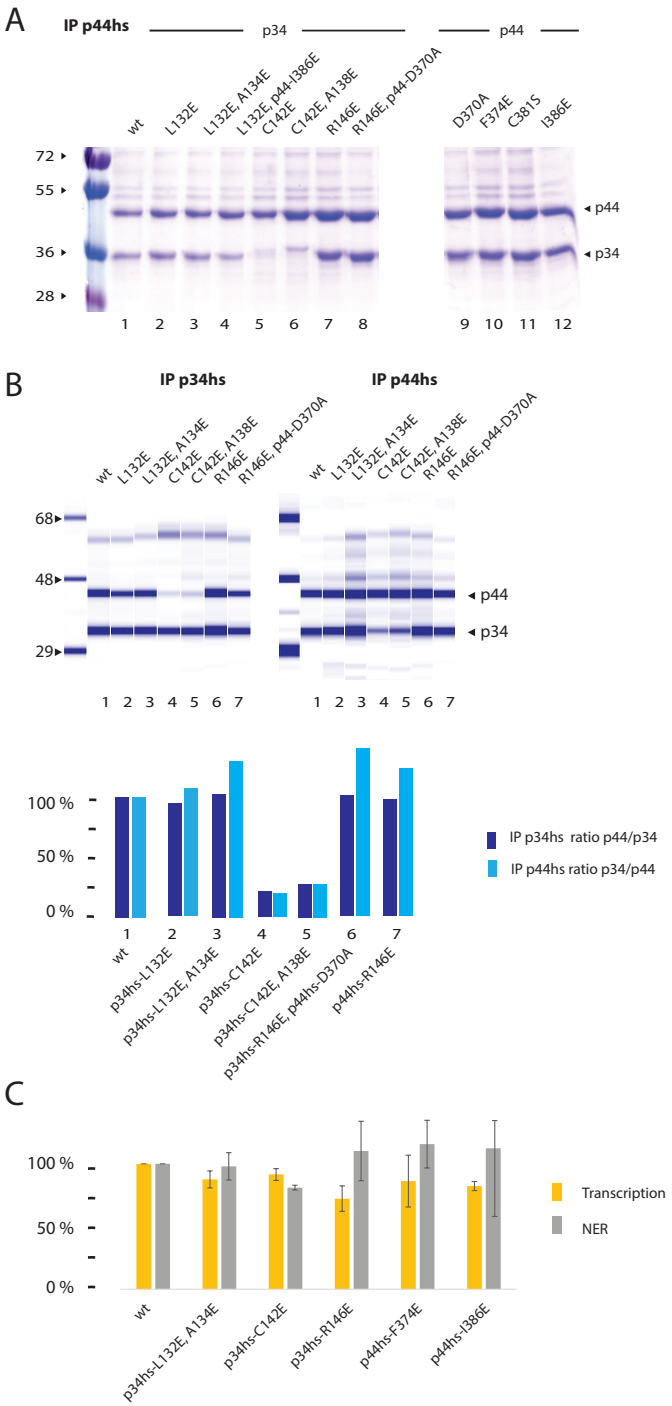

Figure S5: Mutational analysis of the interface between full length p34hs/p44hs. Full length wild-type or variants p34hs and p44hs were co-expressed in insect cells and the association of the two proteins was analysed using pull down experiments directed against p34hs (using strep-tag affinity) or p44hs (using the 1H5 monoclonal antibody directed against p44hs) **(A**) SDS-PAGE analysis followed by Coomassie staining of the pull-down experiments using p44hs as bait (IP p44hs) **(B)** Quantification of the pull down analysis using capillary electrophoresis (IP p34hs and IP p44hs). **(C)** Quantification of the NER and transcription activity of core-TFIIH harbouring mutations in p34hs or p44hs from Figures 3E and 3F. Activities from independent experiments (n=3 and n=2, respectively) were normalized to wild-type and averaged.

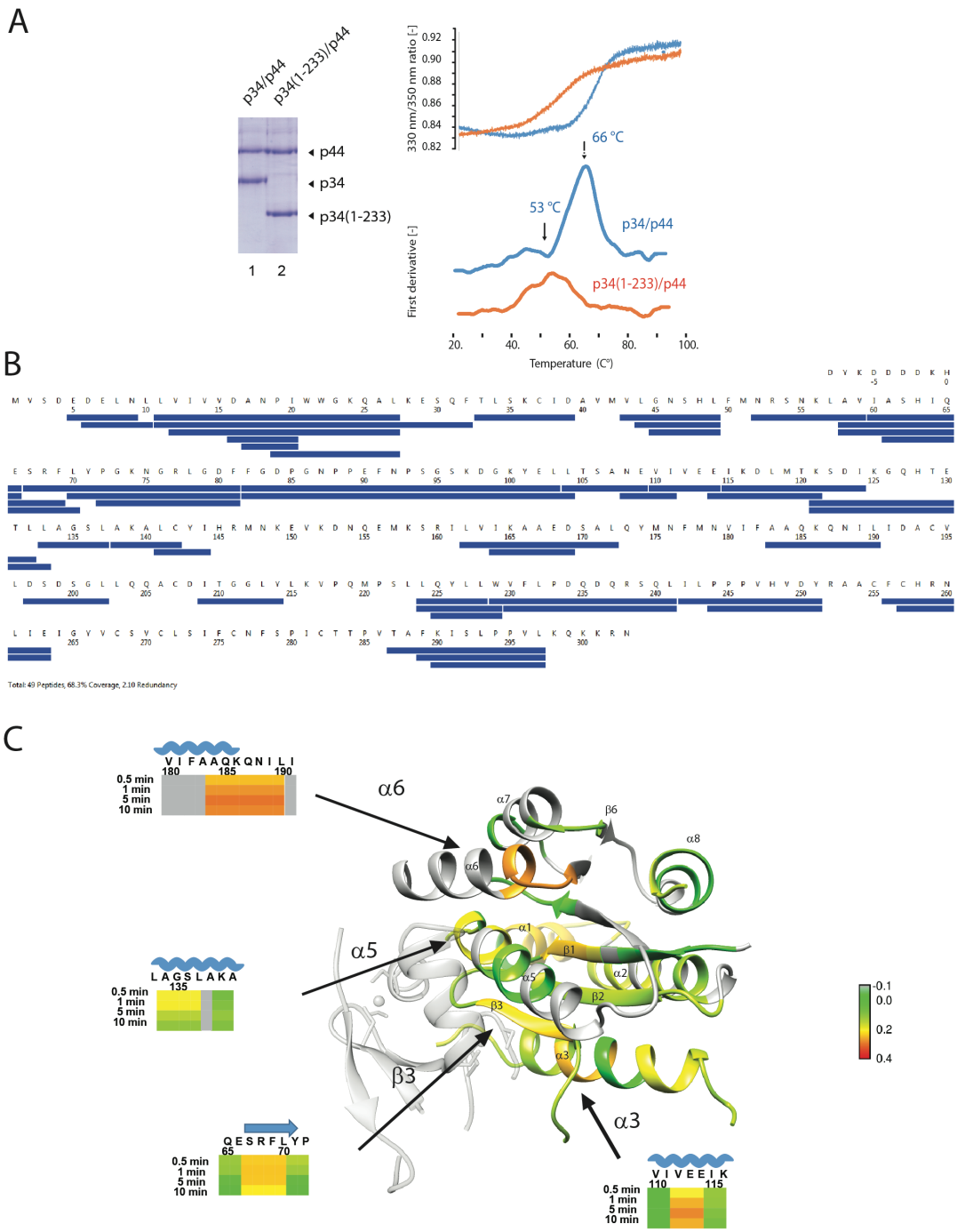

Figure S6: Stability of the p34/p44 heterodimer and HDMX analysis. **(A**) Full length strep-tagged p34hs or p34hs(1-233) and p44hs were co-expressed in insect cells and the complex was purified using strep-tag affinity chromatography. Purified complexes (left panel) were analysed using the NanoTemper Technologies Prometheus instrument to evaluate their thermal stability (right panel). (**B and C**) Hydrogen-Deuterium eXchange coupled to Mass Spectrometry experiments in which the deuterium exchange labelling of p34hs full length in the presence and absence of p44hs was compared. The sequence coverage of p34hs is shown in Figure **(B).** Mapping of the measured backbone amide deuterium uptake after 30 sec, 1 min, 5 min and 10 min on the 3D structure of the p34hs vWA domain is illustrated in **(C)**.

A

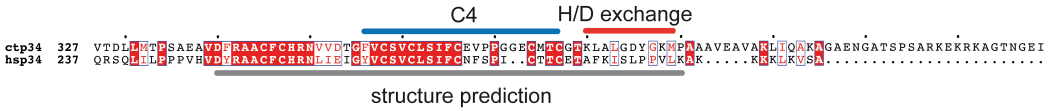

B

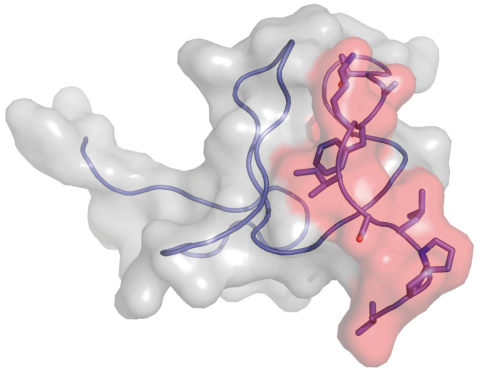

Figure S7: C4 domain model of p34hs **(A)** Sequence alignment of the C4 domains of p34ct and p34hs. The alignment was prepared using Clustal omega and colored with the ESPRIPT server. **(B)** Model of the C4 domain of p34hs. The structure is depicted in ribbon mode with a transparent surface. The area that shows the lowest deuterium exchange rate in the C4 domain is labeled in red and the residues are depicted in stick mode. The model was prepared using the Phyre2 server and manual corrections of the model were made in coot.

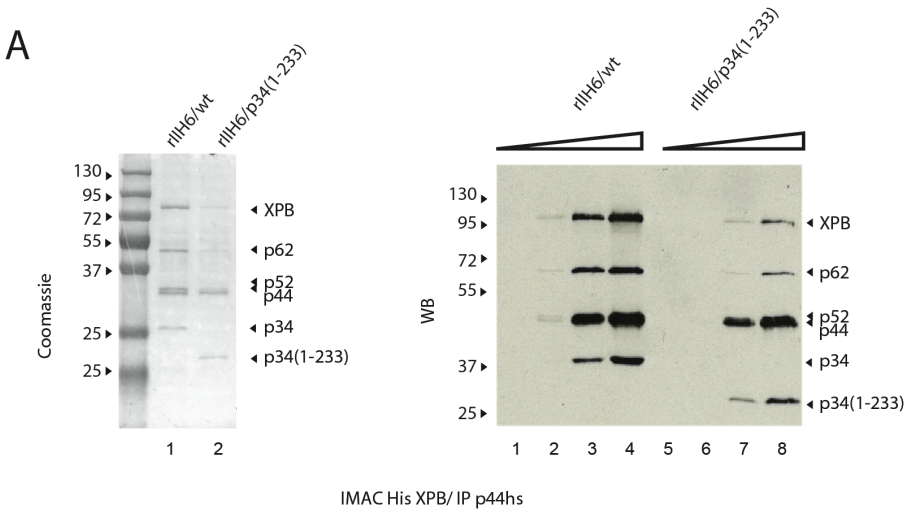

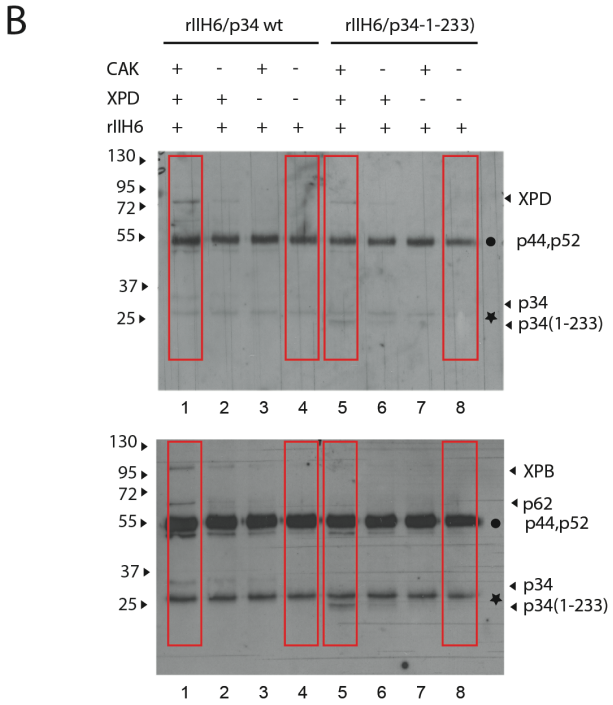

Figure S8: Influence of the p34hs C-terminal domain on the integrity of TFIIH. **(A)** Extracts from 200 10^6 Sf9 cells co-infected by viruses expressing core-TFIIH wild-type (rIIH6/p34 wt) or mutant (rIIH6/p34(1-233)) were purified using IMAC affinity chromatography followed by immune-precipitation with an anti-p44 antibody. Purified proteins were resolved by SDS-PAGE followed by Coomassie staining where 5 µl of the eluate were analyzed (1/40 of total) (left panel) or by immune detection using specific antibodies where 0.1, 0.3, 1.0 and 3.0 µl of the eluate were loaded on the gel (right panel). **(B)** Extracts of SF9 cells co-infected by viruses expressing core-TFIIH wild-type (rIIH6/p34 wt) or mutant (rIIH6/p34(1-233)) were incubated with XPD plus CAK, immuno-precipitated using an antibody directed against cdk7 and immobilized proteins were analyzed using specific antibodies. Heavy (black circle) and light chains (black star) of the anti-cdk7 antibody are indicated. Lanes 1, 4, 5 and 8 have been used in Figure 4D.

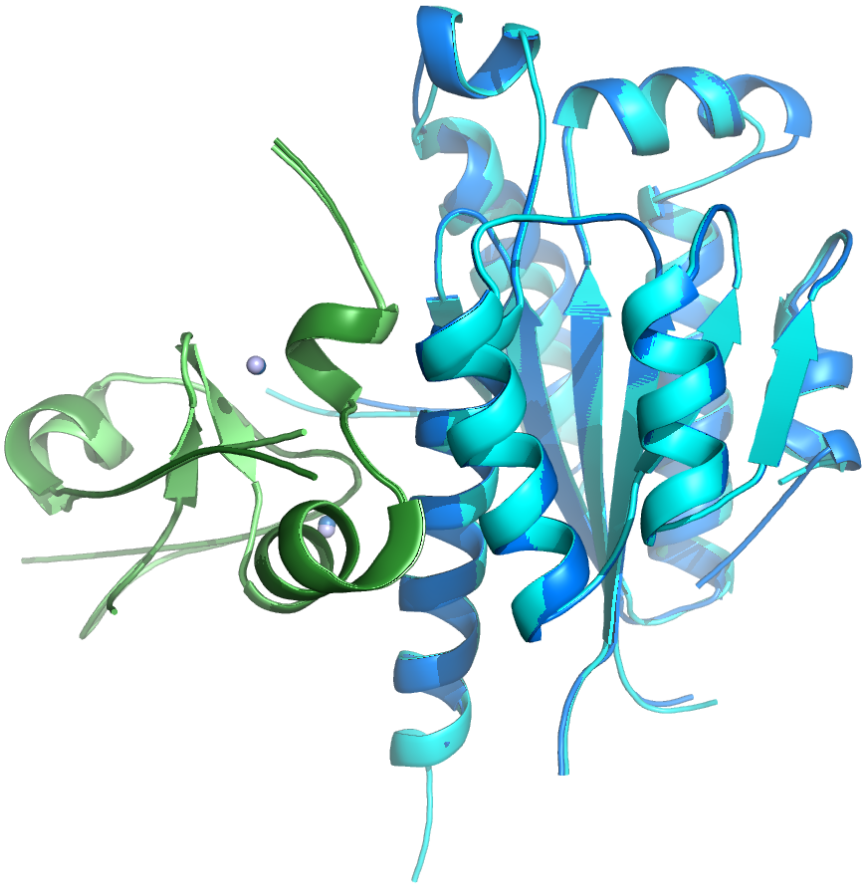

Figure S9: Superposition of the p34ct/p44ct complex I (in dark blue and dark green for p34 and p44, respectively) and the p34ct/p44ct complex II (in cyan and light green for p34 and p44, respectively). The blue spheres represent the Zn ions.

Table S1

TFIIH	Human	EM RTC	Schultz et al., Cell 2000	PMID:	11007478
TFIIH core	Saccharomyces cerevisiae	EM 2D	Chang et al., Cell 2000	PMID:	11007479
TFIIH	Trypanosoma brucei	EM RTC	Lee et al., NAR 2009	PMID:	19386623
TFIIH	Saccharomyces cerevisiae	EM RTC	Gibbons et al., PNAS 2011	PMID:	22308316
Pol II PIC	Saccharomyces cerevisiae	Cryo-EM	Murakami et al., Science 2013	PMID:	24072820
Pol II Med PIC	Saccharomyces cerevisiae	Cryo-EM	Robinson et al., Cell 2016	PMID:	27610567
Pol II PIC	Human	Cryo-EM	He et al., Nature 2012	PMID:	23446344
Pol II PIC	Human	Cryo-EM	He et al., Nature 2016	PMID:	27193682

XPB	Human	4ERN	Hilario et al Acta D, 2013	PMID:	23385459
XPB	*Archeoglobus fulgidus*	*2FWR*	*Fan et al., Mol Cell, 2006*	*PMID:*	*16600867*
XPB	*Archeoglobus fulgidus*	*2FZ4*	*Fan et al., Mol Cell, 2006*	*PMID:*	*16600867*
XPB	*Archeoglobus fulgidus*	*2FZL*	*Fan et al., Mol Cell, 2006*	*PMID:*	*16600867*
p62	Human	1PFJ	Gervais et al., 2004	PMID:	15195146
p62	Human	2RNR	Okuda et al., EMBO 2008	PMID:	18354501
p62	Human	2RUK	Okuda et al., JACS 2014	PMID:	25216154
p62	Human	2DII	Not published	na	na
p62	Saccharomyces cerevisiae	2LOX	Lafrance-Vanasse et al., NAR 2012	PMID:	22373916
p62	Saccharomyces cerevisiae	2M14	Lafrance-Vanasse et al., NAR 2013	PMID:	23295669
p62	Saccharomyces cerevisiae	1Y5O	Di Lello et al., Biochemistry 2005	PMID:	15909982
p62	Saccharomyces cerevisiae	2GS0	Di Lello et al., Mol Cell 2006	PMID:	16793543
p62	Saccharomyces cerevisiae	2K2U	Langlois et al., JACS 2008	PMID:	18630911
p62	Saccharomyces cerevisiae	2L2I	Mas et al., to be published	na	na
p62	Saccharomyces cerevisiae	2MKR	Chabot et al., Plos Path 2014	PMID:	24675874
p8/p52	Saccharomyces cerevisiae	3DOM	Kainov et al., NSBM 2008	PMID:	19172752
p8/p52	Saccharomyces cerevisiae	3DGP	Kainov et al., NSBM 2008	PMID:	19172752
p34	Chaetomium themophilum	4PN7	Schmitt et al., PlosOne 2014	PMID:	25013903
p34/p44	Human	na	This work	na	na
p44	Human	1Z60	Kelleberger et al., 2006	PMID:	15790571
p8	Human	2JNJ	Vitorino et al., J Mol Biol 2007	PMID:	17350038
p8	Human	1YDL	na	PMID:	na
p8/p52	Saccharomyces cerevisiae	3DOM	Kainov et al., NSBM 2008	PMID:	19172752
p8/p52	Saccharomyces cerevisiae	3DGP	Kainov et al., NSBM 2008	PMID:	19172752
XPD	*Thermoplasma acidophilum*	*4A15*	*Kuper et al., EMBO 2011*	*PMID:*	*22081108*
XPD	*Thermoplasma acidophilum*	*2VSF*	*Kuper et al., Plos Biol 2008*	*PMID:*	*18578568*
XPD	*Sulfolobus acidocaldarius*	*3CRV*	*Fan et al., Cell 2008*	*PMID:*	*18510924*
XPD	*Sulfolobus tokodaii*	*2VL7*	*Liu et al., Cell 2008*	*PMID:*	*18510925*
CDK7	Human	1UA2	Lolli et al, Structure 2004	PMID:	15530371
cyclin H	Human	1JKW	Andersen et al., EMBO 1997	PMID:	9118957
cyclin H	Human	1KXU	Kim et al., NSBM 1996	PMID:	8836101
MAT1	Human	1G25	Gervais et al., JBC 2000	PMID:	11056162

Table S1. Published structures of TFIIH and complexes of subunits determined by EM, X-ray crystallography and NMR.

Table S2

	p34hs	HS	ASA	BSA	(%)		p34ct	HS	ASA	BSA	(%)		ALIGNED
	LEU 57		0	0	0		VAL 68		4	0	0		
	ALA 58		0	0	0		ALA 69		0	0	0		
	VAL 59		0	0	0		ILE 70		0	0	0		
	ILE 60		0	0	0		ILE 71		0	0	0		
	ALA 61		0	0	0		ALA 72		0	0	0		
	SER 62		0	0	0		SER 73		0	0	0		
	HIS 63		0	0	0		HIS 74		0	0	0		
	ILE 64		4	0	0		THR 75		5	0	0		
	GLN 65		46	22	50	POL	ASN 76	H	96	59	70	POL	1
	GLU 66		55	9	20	CH	ARG 77		60	53	90	CH	1
	SER 67	H	7	5	70	POL	ALA 78	H	23	20	90	APOL	1
	ARG 68		40	2	10	CH	VAL 79		56	1	10	APOL	
	PHE 69		47	44	10	APOL	TRP 80	H	51	41	90	APOL	1
	LEU 70		0	0	0		LEU 81		0	0	0		
	TYR 71		37	0	0		TYR 82		6	0	0		
1	PRO 72	H	20	3	20	APOL	PRO 83		23	14	70	APOL	1
	GLY 73		31	4	20	APOL	GLN 84		89	4	10	POL	1
	LYS 74		157	69	50	CH	PRO 85		86	10	20	APOL	
	GLY 75		125	6	10	APOL	PRO 86		117	84	80	APOL	1
							GLU 87		117	19	20	CH	
							PRO 88		153	16	20	APOL	
							ALA 89		117	7	10	APOL	
	ILE 115		14	0	0		LEU 126		12	0	0		
	LYS 116		130	0	0		MET 127		51	0	0		
	ASP 117		58	0	0		ASP 128		121	0	0		
	LEU 118		0	0	0		ASP 129	HS	85	14	20	CH	
	MET 119		63	0	0		THR 130		32	0	0		
	THR 120		116	0	0		THR 131		65	0	0		
	LYS 121		86	0	0		PRO 132		108	0	0		
	SER 122		37	0	0		SER 133		74	0	0		
	ASP 123		86	0	0		ASP 134		1	0	0		
	ILE 124		154	0	0		LEU 135		87	0	0		
	GLN 127		129	30	30	POL	ASP 136		98	0	0		
	HIS 128		118	3	10	CH	THR 137		39	0	0		
	THR 129		87	0	0		THR 138		94	0	0		
	GLU 130		48	0	0		THR 139		32	0	0		
	THR 131		10	0	0		THR 140		11	0	0		
	LEU 132		57	34	60	APOL	GLN 141	H	45	34	80	POL	1
	LEU 133		9	0	0		ILE 142		3	0	0		
	ALA 134		15	8	60	APOL	SER 143	H	6	5	90	POL	1
1	GLY 135		30	30	100	APOL	GLY 144		22	22	100	APOL	1
	SER 136		0	0	0		ALA 145		0	0	0		
	LEU 137		2	0	0		LEU 146		0	0	0		
	ALA 138		44	43	10	APOL	THR 147	H	79	79	100	POL	1
	LYS 139		76	65	9	CH	LEU 148		58	56	100	APOL	1
	ALA 140		0	0	0		ALA 149		0	0	0		
1	LEU 141		16	15	10	APOL	LEU 150		20	18	90	APOL	1
	CYS 142	H	73	65	9	POL	ALA 151		58	58	100	APOL	1
	TYR 143		11	10	10	APOL	HIS 152		44	26	60	CH	1
	ILE 144		2	0	0		ILE 153		6	0	0		
	HIS 145		96	70	80	CH	ASN 154	H	86	51	60	POL	1
	ARG 146	H	89	59	70	CH	LYS 155	HS	141	97	70	CH	1
	MET 147		8	0	0		THR 156		24	0	0		
	ASN 148		56	0	0		ALA 157		35	0	0		
	LYS 149		129	19	20	CH	LEU 158		108	28	30	APOL	
	GLU 150		99	0	0		SER 159		69	0	0		
	VAL 151		42	0	0		LEU 160		42	0	0		
	LYS 152		104	0	0		THR 161		91	0	0		
	ASP 153		112	0	0		ALA 162		66	0	0		
	ASN 154		137	0	0		SER 163		83	0	0		
	GLN 155		54	0	0		ASN 164		84	0	0		
	GLU 156		127	0	0		THR 165		88	0	0		
	MET 157		26	0	0		ALA 166		162	0	0		
	LYS 158		83	0	0		ALA 198		102	0	0		
	SER 159		9	0	0		GLY 199		41	0	0		
	ARG 160		51	0	0		LEU 200		34	0	0		
	ILE 161		1	0	0		HIS 201		115	0	0		
	LEU 162		5	0	0		ALA 202		13	0	0		
	VAL 163		0	0	0		ARG 203		90	0	0		
	ILE 164		2	0	0		ILE 204		0	0	0		
	LYS 165		0	0	0		LEU 205		0	0	0		
	ALA 166		0	0	0		ILE 206		0	0	0		
	ALA 167		3	0	0		ILE 207		0	0	0		
	GLU 168		116	0	0		SER 208		2	0	0		
	ASP 169		45	0	0		VAL 209		0	0	0		
							SER 210		5	0	0		
							ASP 211		49	0	0		
							SER 212		18	0	0		
							SER 213		31	0	0		
							ALA 214		84	0	0		
	LEU 172		158	0	0		ALA 215		91	0	0		
	GLN 173		93	0	0		GLN 216	H	49	22	50	POL	
	TYR 174		103	0	0		TYR 217		93	0	0		
	MET 175		110	0	0		ILE 218		126	5	10	APOL	
	ASN 176		82	56	70	POL	PRO 219	H	48	31	70	APOL	1
	PHE 177		1	0	0		THR 220		1	0	0		
	MET 178		75	0	0		MET 221		20	0	0		
1	ASN 179	H	83	52	70	POL	ASN 222	H	89	71	80	POL	1
	VAL 180		13	13	100	APOL	ALA 223		6	6	100	APOL	1
	ILE 181		5	0	0		VAL 224		1	0	0		
	PHE 182		58	0	0		PHE 225		111	0	0		
1	ALA 183		44	41	100	APOL	ALA 226		47	44	100	APOL	1
	ALA 184		0	0	0		ALA 227		0	0	0		
	GLN 185		76	0	0		ALA 228		27	0	0		
	LYS 186		178	0	0		HIS 229		161	21	20	POL	1
	GLN 187		78	18	30	POL	ALA 230		57	1	10	APOL	
	ASN 188		111	0	0		ARG 231		216	0	0		
	ILE 189		2	0	0		ILE 232		12	0	0		

Table S3

Hs p44	HSDC	ASA	BSA	BSAS		Ct p44	HSDC	ASA	BSA	BSAS		ALIGNED
						PHE 380		194	23	20	APOL	
						PRO 381		131	0	0		
						LEU 382		45	0	0		
PRO 327		194	0	0		LYS 383		138	0	0		
LEU 328		117	0	0		GLY 384		46	0	0		
ASP 329		81	0	0		TRP 385		23	0	0		
ALA 330		64	0	0		VAL 386		81	0	0		
PHE 331		26	0	0		GLU 387		68	0	0		
GLN 332		103	0	0		VAL 388		4	0	0		
GLU 333		90	0	0		SER 389		64	0	0		
ILE 334		34	0	0		TRP 390		70	0	0		
PRO 335		53	0	0		ALA 391		76	0	0		
LEU 336		149	0	0		GLU 392		67	0	0		
ASP 337		123	0	0		ALA 393		7	0	0		
GLU 338		93	0	0		ARG 394		208	0	0		
TYR 339		143	0	0		LYS 395		175	0	0		
ASN 340		115	0	0		SER 396		34	0	0		
GLY 341		57	0	0		LYS 397		190	0	10	CH	
GLU 342		34	0	0		GLN 398		39	0	0		
ARG 343		191	0	0		VAL 399		114	77	70	APOL	
PHE 344		110	34	40	APOL	GLY 400		18	12	70	APOL	1
CYS 345		5	0	0		CYS 401		1	0	40	POL	
TYR 346		91	32	40	APOL	PHE 402		71	19	30	APOL	1
GLY 347		45	45	100	APOL	ALA 403	H	42	42	100	APOL	1
CYS 348	H	73	73	100	POL	CYS 404		67	59	90	POL	1 1
GLN 349	H	156	113	80	POL	LEU 405		141	122	90	APOL	1
GLY 350		19	14	80	APOL	ALA 406		41	15	40	APOL	1
GLU 351		161	0	0		PRO 407		108	11	20	APOL	
VAL 357		37	0	0		PHE 408		20	0	0		
TYR 358		52	0	0								
LYS 359		75	0	0								
CYS 360		3	0	0		CYS 476		2	0	0		
ALA 361		52	0	0		PRO 477		67	0	0		
VAL 362		67	0	0		THR 478		99	0	0		
CYS 363		29	0	0		CYS 479		40	0	0		
GLN 364		161	0	0		GLY 480		30	0	0		
ASN 365		50	0	0		LYS 481		53	0	0		
VAL 366		27	0	0		HIS 482		7	0	0		
PHE 367		5	0	0		PHE 483		0	0	0		
CYS 368		27	2	10	POL	CYS 484	H	21	8	40	POL	
VAL 369		89	0	0		ILE 485		89	1	10	APOL	
ASP 370		110	59	60	CH	ASP 486	HS	107	64	70	CH	1 1
CYS 371		21	20	100	POL	CYS 487		17	15	100	POL	1 1
ASP 372		17	0	0		ASP 488		22	0	0		
VAL 373		77	5	10	APOL	VAL 489		73	0	0		
PHE 374		107	104	100	APOL	PHE 490		100	83	90	APOL	1 1
VAL 375		8	3	40	APOL	ALA 491		0	0	0		
HIS 376		33	0	0		HIS 492		49	0	0		
ASP 377		83	0	0		GLU 493		122	0	0		
SER 378		67	20	30	POL	VAL 494		94	45	50	APOL	1
LEU 379		77	73	100	APOL	ILE 495		83	83	100	APOL	1
HIS 380		122	16	20	CH	HIS 496	H	61	10	20	CH	1 1
SER 381	H	51	33	70	POL	ASN 497	H	64	60	100	POL	1
CYS 382		13	0	0		CYS 498		2	0	0		
PRO 383		33	31	100	APOL	PRO 499		36	35	100	APOL	1 1
GLY 384		5	0	0		GLY 500		0	0	0		
CYS 385		42	0	0		CYS 501		26	0	0		
ILE 386		123	95	80	APOL	GLN 502	H	105	79	80	POL	1
HIS 387	H	123	112	100	CH	ALA 503	H	72	70	100	APOL	1
						ASP 504		53	6	20	CH	
LYS 388		225	36	20	CH	MET 505	H	151	59	40	APOL	1
						ARG 506	HS	191	79	50	CH	
						PRO 507		189	2	10	APOL	

Tables S2 and S3. Structural alignment of human and Ct p34 vWA domains and p44 RING fingers. Interfaces were analysed with PISA (http://pdbe.org/pisa/). HS (residues making Hydrogen bonds or Salt bridges), ASA (Accessible Surface Area, Å^2), BSA (Buried Surface Area, Å^2 and %). Residues in the Table are color coded: Interfacial residues in gold or yellow (according to their BSA, above or below 50%), buried in light blue and exposed in grey. Aligned interface residues are indicated by an orange or a red box (when identical).